

# FreeOrbit4D: Training-Free Arbitrary Camera Redirection for Monocular Videos via Geometry-Complete 4D Reconstruction

Wei Cao<sup>1</sup> Hao Zhang<sup>1</sup> Fengrui Tian<sup>2</sup> Yulun Wu<sup>1</sup>  
 Yingying Li<sup>1</sup> Shenlong Wang<sup>1</sup> Ning Yu<sup>3</sup> Yaoyao Liu<sup>1</sup>

<sup>1</sup>University of Illinois Urbana-Champaign <sup>2</sup>University of Pennsylvania <sup>3</sup>Eyeline Labs

{weicao3, haoz19, yulun5, yl101, shenlong, lyy}@illinois.edu tianfr@upenn.edu ning.yu@scanlinevfx.com

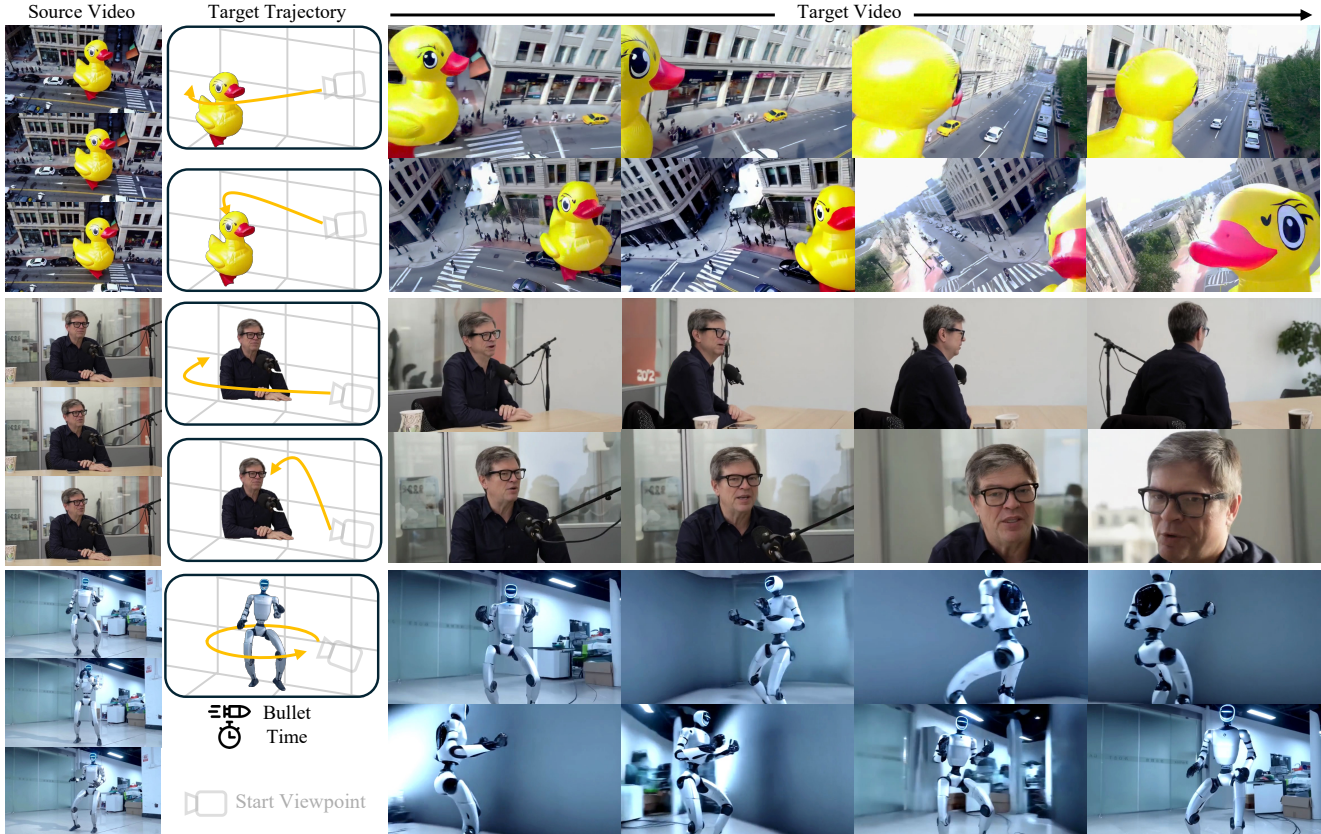


Figure 1. FreeOrbit4D enables **training-free** camera redirection from a single monocular video to arbitrary target camera trajectories. Given a source video (left) and a target trajectory (middle), our method produces a redirected video (right) with faithful appearance and strong temporal coherence under large-angle redirected camera motions, even including bullet-time orbits, demonstrated on diverse scenes and subjects.

## Abstract

*Camera redirection aims to replay a dynamic scene from a single monocular video under a user-specified camera trajectory. However, large-angle redirection is inherently ill-posed: a monocular video captures only a narrow spatio-*

*temporal view of a dynamic 3D scene, providing highly partial observations of the underlying 4D world. The key challenge is therefore to recover a complete and coherent plenoptic representation from this limited input, with consistent geometry and coherent motion. While recent diffusion-based methods achieve impressive visual genera-*

tion quality, they often break down under large-angle viewpoint changes far from the original trajectory, where missing visual grounding leads to severe geometric ambiguity and temporal inconsistency. To address this, we present **FreeOrbit4D**, an effective training-free framework that tackles this geometric ambiguity by recovering a geometry-complete 4D proxy as structural grounding for video generation. We obtain this proxy by decoupling foreground and background reconstructions: we unproject the monocular video into a static background and geometry-incomplete foreground point clouds in a unified global space, then leverage an object-centric multi-view diffusion model to synthesize multi-view images and reconstruct geometry-complete foreground point clouds in canonical object space. By aligning the canonical foreground point cloud to the global scene space via dense pixel-synchronized 3D–3D correspondences and projecting the geometry-complete 4D proxy onto target camera viewpoints, we provide geometric scaffolds (e.g., depth/visibility cues) that guide a conditional video diffusion model. Extensive experiments show that **FreeOrbit4D** produces more faithful and temporally coherent redirected videos under challenging large-angle trajectories, and our geometry-complete 4D proxy further opens a potential avenue for practical applications such as edit propagation and 4D data generation. **Project page and code will be released soon.**

## 1. Introduction

Camera redirection seeks to endow machines with the ability to synthesize novel video sequences from a source video along a user-specified camera trajectory [3, 11, 13, 47]. For example, consider the video interview footage in Fig. 1. Although recorded from a fixed viewpoint, we can easily imagine the same scene from the side, back, or top-down, by mentally reconstructing a consistent 3D world and replaying its dynamics from a virtual perspective. Enabling machines to perform this same task is central to applications such as Autonomous Driving [7, 52, 53], AR/VR [1], and cinematic effects like bullet-time replay from limited camera setups [9, 34, 48]. Today, in industry, such effects rely on costly multi-camera rigs and multi-view reconstruction techniques [18, 25]; enabling free-viewpoint camera redirection from a single video would democratize these experiences for everyday capture.

However, camera redirection from a single monocular video is inherently ill-posed. A monocular video captures only a narrow spatio-temporal view of a dynamic 3D scene, providing highly partial observations of the underlying 4D world. The key challenge is to recover a complete and coherent plenoptic representation from this limited input, with consistent geometry and coherent motion. While prior methods can interpolate nearby novel views by reconstruct-

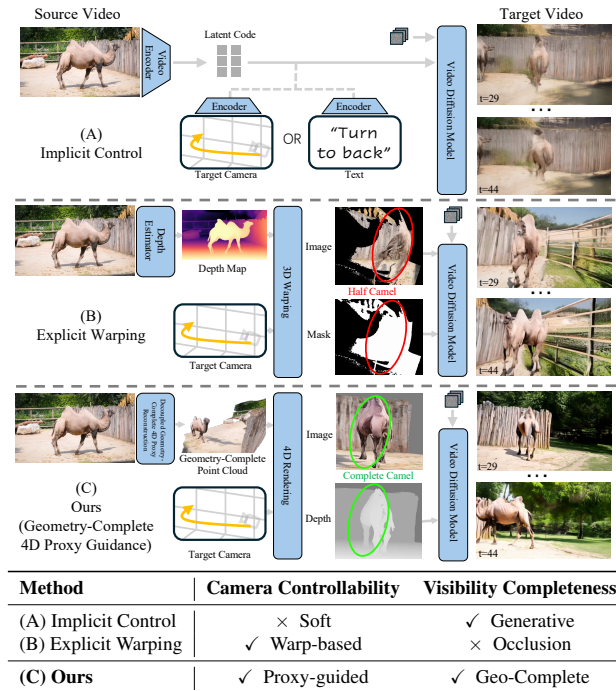


**Figure 2. Comparison of video camera redirection paradigms.** We compare 3 representative approaches for camera redirection from monocular video. **(A) Implicit Control:** Camera motion is specified via learned embeddings. Such implicit representations provide only soft controllability: text cannot precisely describe complex trajectories, and learned conditions often fail to follow the intended path (e.g., the “turn to back” instruction). Moreover, training requires paired data, which is expensive and scarce. **(B) Explicit Warping:** These methods warp observed pixels to target viewpoints using estimated depth. However, occluded regions remain unfilled, producing visible holes (red circles show “Half Camel”). **(C) Ours:** We reconstruct a geometry-complete 4D proxy that recovers both visible and occluded surfaces, then render it from target viewpoints as geometric guidance for video generation. This enables precise camera control with complete visibility from arbitrary viewpoints (green circle shows “Complete Camel”). The table below summarizes key trade-offs across camera controllability and visibility completeness. ✓, and ✗ denote full and lack of support.

ing observed surfaces [5, 18, 25, 34], they break down under large-angle viewpoint changes far from the original camera trajectory. In these regimes, the absence of visual grounding introduces severe geometric ambiguity, fundamentally limiting replay from arbitrary viewpoints.

To tackle the challenge, recent studies [3, 13, 14, 21, 23, 24, 31, 46, 47] try to explore the generative power of video foundation models for camera redirection. As shown in Fig. 2, these methods generally follow two paradigms: implicit control and explicit warping. Implicit control methods [3, 11, 13] encode camera trajectories as learned embed-

dings [3, 11, 13] or text prompts [39] and inject them into video diffusion models; however, such implicit representations offer only soft controllability and require expensive 4D training data. Explicit warping methods [14, 31, 46] instead estimate depth and warp observed pixels to target viewpoints, but since only visible surfaces are available, occluded regions produce unfilled holes that must be hallucinated by downstream generators [39, 44]. Neither paradigm achieves both precise camera control and complete visibility of unseen regions, which are essential for faithful large-angle camera redirection.

In this paper, we propose FreeOrbit4D, an effective training-free framework for arbitrary camera redirection from a single monocular video via geometry-complete 4D reconstruction. Our key idea is to explicitly reason about and recover a complete 4D geometry from partial monocular observations, and to use this geometry as structural guidance for generative rendering at novel viewpoints. By completing the geometry of unseen regions, our method resolves the ambiguity that causes artifacts in prior approaches, enabling consistent video synthesis even when the target trajectory deviates significantly from the original viewpoints. Specifically, we observe that reconstructing dynamic scenes from monocular video and completing occluded object geometry are fundamentally different tasks: the former requires temporally consistent scene-level reasoning, while the latter demands multi-view understanding of object shape. This motivates handling them in distinct representation spaces: we unproject the source video into a global scene space with geometry-incomplete foreground, and complete the foreground geometry via multi-view synthesis in canonical object space. While this separation yields tractable sub-tasks addressable by existing techniques [40, 43, 54], the key challenge lies in unifying their outputs into a coherent whole. Our correspondence-aware alignment addresses this by bridging canonical and global spaces through dense pixel-synchronized 3D–3D correspondences, producing a unified geometry-complete 4D proxy without task-specific training. To interface this proxy with a video generator, we distill it into view-dependent depth maps as conditioning [39]. While depth is not full geometry, it compactly captures metric layout and visibility cues that enforce cross-view and temporal consistency. This conditioning enables faithful large-angle view synthesis and paves the way for potential 4D data generation.

Our contributions are summarized as follows:

- We present a training-free method that achieves geometry-complete 4D reconstruction from monocular video by combining global scene lifting with object geometry completion through dense 3D correspondences.
- Building on this reconstruction, we propose a camera redirection framework tailored for large-angle view synthesis, enabling expansive camera motions with strong geometric consistency across time and viewpoints.

## 2. Related Work

**Camera-controlled video generation.** With the rapid development of video foundation models [4, 19, 33], research has progressed from pure text-to-video generation toward controllable video synthesis with multiple conditioning signals [2, 41, 49]. Among these directions, camera-controlled video generation has attracted increasing attention due to its relevance to downstream video creation applications. Early approaches encode camera intrinsics and extrinsics as control signals [38, 41], but subsequent studies show that such low-dimensional parameters are difficult to exploit effectively in high-dimensional attention-based diffusion models. This has motivated the development of alternative camera representations, including Plücker coordinates [8, 11, 50] and PRope [15, 20], together with diverse control injection mechanisms [3, 11, 15, 23, 41]. Despite promising results enabled by powerful diffusion priors, these methods often struggle to faithfully follow prescribed camera trajectories (Fig. 3) due to the absence of explicit geometric constraints. In contrast, our approach achieves precise camera redirection by explicitly reconstructing and completing 4D scene geometry.

**Reconstruction-grounded 4D generation.** Beyond camera-based video generation, another line of work [6, 13, 21, 22, 32, 36, 46, 47, 51] leverages explicit 4D scene representations to guide camera control. These methods reconstruct a 4D representation from monocular videos using NeRF [25, 34, 35] or Gaussian Splatting [18], render partial videos from novel viewpoints, and rely on video diffusion models to inpaint or outpaint missing regions. While the generative prior enables plausible completion of occluded content, the underlying geometry remains limited to observed surfaces, making it difficult to recover complete 3D structure for dynamic scenes. As a result, such methods struggle with large-angle camera redirection (Fig. 3), limiting their applicability in real-world scenarios. In contrast, our method addresses this limitation by constructing a geometry-complete 4D scene via correspondence-aware alignment.

## 3. Method

In this work, we study the camera redirection task: Given a monocular source video  $\mathcal{V}^{src}$  and a target camera trajectory,

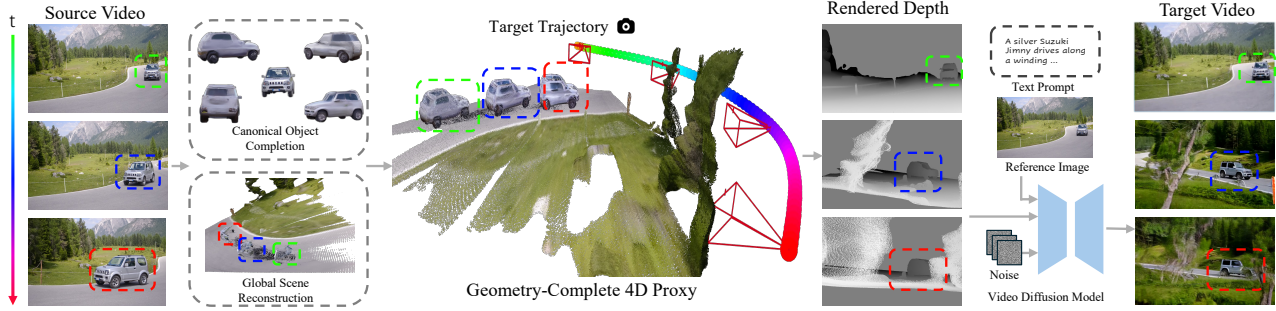


Figure 3. **Overview of FreeOrbit4D.** Our framework redirects a monocular video to a target camera trajectory via a geometry-complete 4D proxy. This proxy is constructed through two branches: *Global Scene Reconstruction* recovers background and partial foreground in global space, while *Canonical Object Completion* reconstructs complete foreground geometry via multi-view synthesis. After alignment, we render view-dependent depth maps from the unified 4D proxy and condition a video diffusion model, along with a reference image and text prompt, enabling faithful novel-view synthesis under large viewpoint changes.

our goal is to synthesize a visually faithful and temporally consistent target video  $\mathcal{V}^{tgt}$  that depicts the same dynamic scene as  $\mathcal{V}^{src}$  but viewed from the target trajectory.

As shown in Fig. 3, our framework has three stages. First, we reconstruct a static background and geometry-incomplete foreground in global scene space, and geometry-complete foreground in canonical object space (Sec. 3.1). Second, we align the canonical foreground to the global scene via dense pixel-synchronized 3D–3D correspondences, yielding a unified geometry-complete 4D proxy (Sec. 3.2). Finally, we render depth scaffolds along the target trajectory and synthesize the output with the video diffusion model (Sec. 3.3).

### 3.1. Decoupled 4D Reconstruction

Since the static scene and the moving object exhibit fundamentally different geometric and motion characteristics, it is natural to decouple their reconstructions. We therefore reconstruct geometry in two complementary coordinate spaces. In **global scene space**, we recover the static background point cloud  $\mathcal{P}^{bg}$  and geometry-incomplete foreground point clouds  $\tilde{\mathcal{P}}_t^{fg}$ , which are lifted from the source frames and thus capture only visible surfaces. In **canonical object space**, we reconstruct geometry-complete foreground point clouds  $\hat{\mathcal{P}}_t^{fg}$  that capture the full 3D structure but lack alignment to the global scene. Throughout, we use tilde ( $\tilde{\cdot}$ ) to denote geometry-incomplete representations in global scene space, and hat ( $\hat{\cdot}$ ) to denote geometry-complete but unaligned representations in canonical object space. These representations will be unified in Sec. 3.2. We detail each branch below.

**Global Scene Reconstruction.** VGGT [40] is a feed-forward model that predicts 3D point maps from images, but assumes a static scene. To handle dynamic videos, we adopt its temporally-aware extension [54], which processes the entire monocular sequence  $\mathcal{V}^{src}$  and predicts temporally

consistent point maps  $\tilde{\mathbf{P}}_t \in \mathbb{R}^{H \times W \times 3}$  for each frame, all registered in a unified global coordinate system.

We then use semantic masks  $\mathbf{M}_t$  from SAM2 [30] to separate background and foreground:

$$\mathcal{P}^{bg} = \bigcup_{t=1}^T \{\tilde{\mathbf{P}}_t(\mathbf{u}) \mid \mathbf{M}_t(\mathbf{u}) = 0\}, \quad (1)$$

$$\tilde{\mathcal{P}}_t^{fg} = \{\tilde{\mathbf{P}}_t(\mathbf{u}) \mid \mathbf{M}_t(\mathbf{u}) = 1\}.$$

Here,  $\mathbf{u}$  denotes pixel coordinates, and  $\tilde{\mathcal{P}}_t^{fg}$  indicates geometry-incomplete foreground point clouds in global scene space, as only visible surfaces are captured from the source viewpoint (visualized as orange in Fig. 4).

**Canonical Object Completion.** To resolve the inherent single-view ambiguity in foreground geometry, we leverage a multi-view video diffusion model [45] to synthesize novel views. Since this model is object-centric and requires isolated object inputs, we first extract the foreground from each frame  $\mathbf{I}_t$  of the source video  $\mathcal{V}^{src}$  using the semantic masks, yielding the masked foreground sequence  $\{\mathbf{I}_t^{fg}\}_{t=1}^T$ . The model then synthesizes four temporally synchronized novel-view videos at  $90^\circ$  azimuthal intervals, denoted as  $\{\mathbf{I}_t^{(k)}\}_{t=1}^T$  for  $k = 1, \dots, 4$ .

We then use VGGT [40] to reconstruct multi-view point maps from all five views (source + four synthesized) per frame:

$$\hat{\mathbf{P}}_t^{fg} = \Phi_{\text{VGGT}} \left( \mathbf{I}_t^{fg}, \mathbf{I}_t^{(1)}, \dots, \mathbf{I}_t^{(4)} \right), \quad \hat{\mathbf{P}}_t^{fg} \in \mathbb{R}^{5 \times H \times W \times 3} \quad (2)$$

where the source view  $\mathbf{I}_t^{fg}$  serves as the reference.  $\hat{\mathbf{P}}_t^{fg}$  resides in canonical object space and requires alignment to the global scene.

Since the synthesized multi-view images contain white backgrounds, the raw point maps include redundant points. We filter them using binary masks: the SAM2 mask  $\mathbf{M}_t$  for the source view, and color thresholding masks  $\{\mathbf{M}_t^{(k)}\}_{k=1}^4$

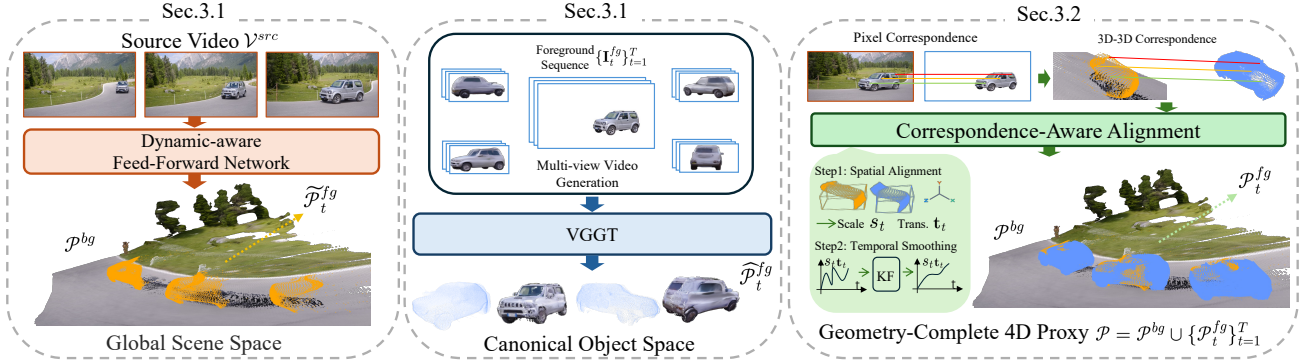


Figure 4. **Decoupled 4D reconstruction and alignment pipeline.** **Left (Sec. 3.1):** A dynamic-aware feed-forward network lifts the source video  $\mathcal{V}^{src}$  into *global scene space*, producing the static background  $\mathcal{P}^{bg}$  and geometry-incomplete foreground  $\tilde{\mathcal{P}}_t^{fg}$  (orange). **Middle (Sec. 3.1):** The foreground sequence  $\{\mathbf{I}_t^{fg}\}_{t=1}^T$  is fed into an object-centric video diffusion model to synthesize multi-view images, from which VGGT reconstructs geometry-complete foreground  $\hat{\mathcal{P}}_t^{fg}$  in *canonical object space*. **Right (Sec. 3.2):** Dense 3D-3D correspondences derived from pixel-synchronized point maps enable *correspondence-aware alignment*: per-frame spatial alignment estimates scale  $s_t$  and translation  $\mathbf{t}_t$ , followed by temporal smoothing via Kalman filtering. The result is the unified geometry-complete 4D proxy  $\mathcal{P} = \mathcal{P}^{bg} \cup \{\mathcal{P}_t^{fg}\}_{t=1}^T$ .

for the novel views. Let  $\hat{\mathbf{P}}_t$  and  $\hat{\mathbf{P}}_t^{(k)}$  denote the point maps for the source and  $k$ -th novel view, respectively. The geometry-complete canonical foreground point cloud is:

$$\begin{aligned} \hat{\mathcal{P}}_t^{fg} = & \{\hat{\mathbf{P}}_t(\mathbf{u}) \mid \mathbf{M}_t(\mathbf{u}) = 1\} \\ & \cup \bigcup_{k=1}^4 \{\hat{\mathbf{P}}_t^{(k)}(\mathbf{u}) \mid \mathbf{M}_t^{(k)}(\mathbf{u}) = 1\} \end{aligned} \quad (3)$$

### 3.2. Correspondence-Aware Alignment

At this stage, we have geometry-incomplete foreground point clouds  $\tilde{\mathcal{P}}_t^{fg}$  in global scene space, and geometry-complete canonical foreground point clouds  $\hat{\mathcal{P}}_t^{fg}$  in canonical object space. Our goal is to align  $\hat{\mathcal{P}}_t^{fg}$  to global scene space, yielding the aligned foreground point clouds  $\mathcal{P}_t^{fg}$ , which together with the static background  $\mathcal{P}^{bg}$  form the unified geometry-complete 4D proxy  $\mathcal{P} = \mathcal{P}^{bg} \cup \{\mathcal{P}_t^{fg}\}_{t=1}^T$ .

**Per-frame Spatial Alignment.** We estimate a per-frame transformation  $\mathcal{T}_t$  such that  $\mathcal{P}_t^{fg} = \mathcal{T}_t(\hat{\mathcal{P}}_t^{fg})$ , using  $\hat{\mathcal{P}}_t^{fg}$  as the spatial anchor. A key observation is that both  $\hat{\mathbf{P}}_t$  and  $\tilde{\mathbf{P}}_t$  originate from the same source image  $\mathbf{I}_t$ , so points at the same pixel  $\mathbf{u}$  correspond to the same surface point. This yields dense 3D-3D correspondences:

$$\mathcal{C}_t = \{(\hat{\mathbf{P}}_t(\mathbf{u}), \tilde{\mathbf{P}}_t(\mathbf{u})) \mid \mathbf{M}_t(\mathbf{u}) = 1\}, \quad (4)$$

which we filter by confidence and outlier removal.

Given  $\mathcal{C}_t$ , a natural approach would be to minimize point-wise distances. However, monocular lifting cannot determine the absolute depth scale, and this scale may vary across frames, causing per-point depth inconsistencies in  $\tilde{\mathcal{P}}_t^{fg}$ . While point-wise fitting would propagate these errors, the overall spatial extent and location of  $\tilde{\mathcal{P}}_t^{fg}$  within

the scene remain reliable. In contrast,  $\hat{\mathcal{P}}_t^{fg}$  provides accurate object geometry from multi-view reconstruction but lacks scene-level positioning. We therefore use  $\hat{\mathcal{P}}_t^{fg}$  only to determine the global placement of the object (position and scale), while preserving the geometry of  $\tilde{\mathcal{P}}_t^{fg}$ . Specifically, we parameterize  $\mathcal{T}_t$  as:  $s_t \mathbf{x} + \mathbf{t}_t$ , where  $(s_t, \mathbf{t}_t)$  are estimated from  $\mathcal{C}_t$  such that the transformed geometry matches the scale and location of  $\tilde{\mathcal{P}}_t^{fg}$ . Rotation is fixed since both reconstructions use the source view as a coordinate reference.

**Temporal Smoothing.** The geo-incomplete foreground  $\tilde{\mathcal{P}}_t^{fg}$  may exhibit frame-to-frame depth inconsistency due to the inherent ambiguity of monocular lifting. Since we use it to anchor global placement, this inconsistency propagates into the aligned foreground trajectory. To compensate, we smooth the centroid trajectory of aligned point clouds using a bidirectional Kalman filter with a constant-velocity motion model, applying stronger regularization along the depth axis. The per-frame scale is preserved to maintain geometric fidelity. This yields a temporally coherent sequence  $\{\mathcal{P}_t^{fg}\}_{t=1}^T$ .

### 3.3. Geometry-conditioned Video Synthesis

Given the geo-complete 4D proxy  $\mathcal{P} = \mathcal{P}^{bg} \cup \{\mathcal{P}_t^{fg}\}_{t=1}^T$  and a target camera trajectory  $\{\pi_t^{tgt}\}_{t=1}^T$ , we render depth scaffolds to guide video synthesis:

$$\mathcal{V}^{tgt} = \Phi_{VDM} \left( \mathbf{I}_1, \{ \text{Render}(\mathcal{P}, \pi_t^{tgt}) \}_{t=1}^T, \mathbf{c} \right), \quad (5)$$

where  $\Phi_{VDM}$  denotes a depth-conditioned video diffusion model [17, 39],  $\mathbf{I}_1$  is the first frame of  $\mathcal{V}^{src}$  serving as appearance reference, and  $\mathbf{c}$  is a text prompt. Depth maps provide a compact yet informative geometric scaffold: they

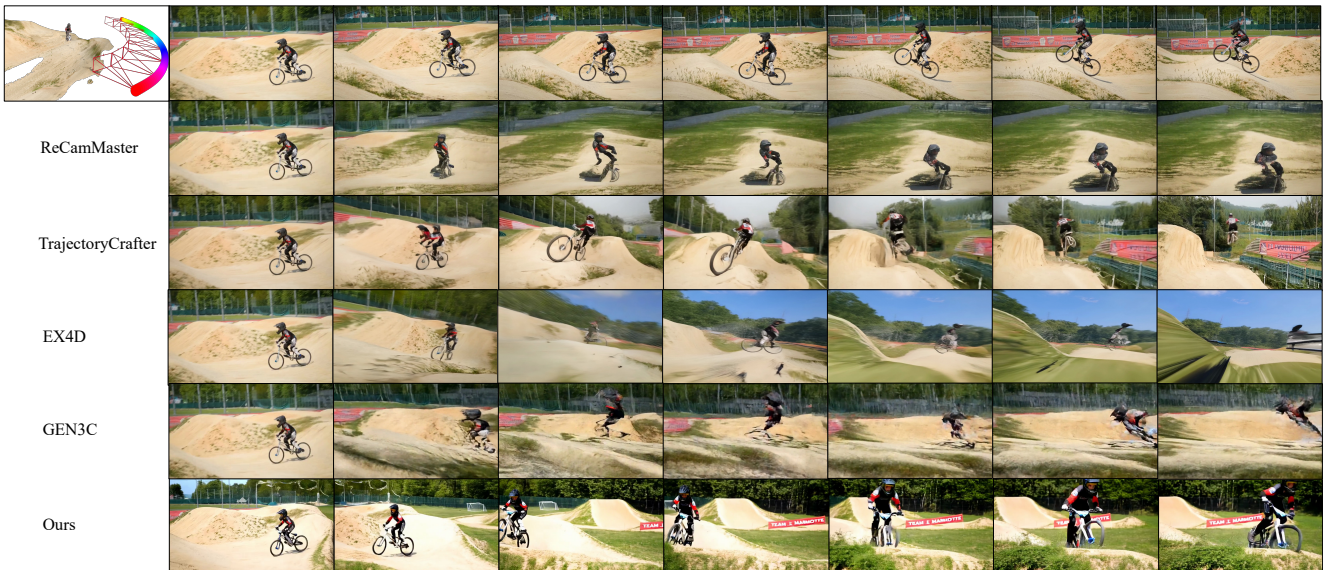


Figure 5. **Qualitative comparison on challenging dynamic sequences: “Swing” (top) and “Bmx” (bottom).** For each sequence, the top-left inset visualizes our reconstructed 4D geometry-complete proxy and the target camera trajectory. These scenarios feature rapid foreground motion, thin structures (e.g., swing ropes), and significant perspective changes. Existing methods exhibit distinct failure modes: ReCamMaster [3] and EX4D [14] suffer from structural disintegration, failing to preserve the integrity of fast-moving subjects (e.g., blurred limbs and ghosting). In contrast, TrajectoryCrafter [46] and GEN3C [31] tend to produce geometric warping and semantic drift, where the background and subjects undergo unnatural distortions as the viewpoint evolves. Our method consistently generates sharp details and stable 4D geometry, effectively handling complex interactions and disocclusions by anchoring pixels to the explicit geometry-complete proxy.

encode the 3D layout from the target viewpoint, allowing video diffusion models to generate spatially coherent content that faithfully follows the prescribed camera motion.

## 4. Experiments and Applications

We evaluate FreeOrbit4D on diverse real-world and synthetic videos under challenging large-angle camera trajectories. After describing implementation details, datasets, and metrics, we compare against state-of-the-art methods (Sec. 4.1), demonstrate practical applications (Sec. 4.2), and

Table 1. **Quantitative comparison and User Study.** We report VBench for perceptual video quality, DINO/CLIP-SIM for semantic similarity, FID-V/FVD-V for distributional fidelity, and user ratings (1–5 scale). **Bold:** best; underline: second-best.

Method	VBench $\uparrow$							Similarity & Fidelity				User Study		
	Subject Consis.	BG Consis.	Motion Smooth.	Overall Consis.	Aesth. Qual.	Imaging Qual.	DINO-SIM $(\uparrow)$	CLIP-SIM $(\uparrow)$	FID-V $(\downarrow \times 10^2)$	FVD-V $(\downarrow \times 10^3)$	Overall $(\uparrow)$	Motion $(\uparrow)$	Stab. $(\uparrow)$	
ReCamMaster	0.84	<u>0.92</u>	<b>0.98</b>	0.16	0.39	43	0.37	0.75	2.6	3.9	2.0	2.5	2.0	
TrajectoryCrafter	0.80	<u>0.91</u>	0.94	<u>0.19</u>	<u>0.47</u>	<u>53</u>	<u>0.47</u>	<u>0.79</u>	<u>2.0</u>	<u>3.6</u>	<u>2.8</u>	3.2	<u>2.9</u>	
EX-4D	0.76	0.89	0.94	0.16	0.42	46	0.28	0.69	3.2	3.8	2.0	2.5	2.0	
GEN3C	0.79	0.88	0.95	0.18	0.42	49	0.43	0.75	2.3	<b>3.3</b>	2.4	<u>3.5</u>	2.3	
<b>Ours</b>	<b>0.88</b>	<b>0.94</b>	<u>0.96</u>	<b>0.24</b>	<b>0.52</b>	<b>64</b>	<b>0.65</b>	<b>0.84</b>	<b>1.7</b>	<u>3.6</u>	<b>4.6</b>	<b>4.5</b>	<b>4.5</b>	

provide ablation studies (Sec. 5).

**Implementation Details.** Our pipeline is training-free and relies on off-the-shelf pretrained models: PAGE-4D [54] for global scene reconstruction, SAM2 [30] for foreground segmentation, SV4D2.0 [45] for multi-view video synthesis, VGGT [40] for multi-view point-map reconstruction, and Wan2.2-VACE [17, 39] for depth-conditioned video synthesis. All experiments are conducted on a single NVIDIA A40 GPU. We process 45 frames per clip at a resolution of  $832 \times 480$ . End-to-end inference takes approximately 50 minutes per video.

**Evaluation Datasets.** We evaluate on a diverse set of real-world and synthetic videos. For real-world data, we use sequences from DAVIS [28], which provides high-quality monocular videos with varied dynamic foregrounds, as well as publicly available online videos (e.g., Unitree robot demos, LeCun interview footage) that feature complex real-world motion and cluttered backgrounds. For synthetic data, we include sequences generated by VEO [10] and Sora [26], covering diverse scenes and motion patterns. To evaluate large-angle camera redirection, we define target trajectories with extreme yaw or pitch rotations (e.g.,  $120^\circ$  or  $180^\circ$ ) from the initial viewpoint.

**Evaluation Metrics.** We evaluate visual quality using FID-V [12] and FVD-V [37], semantic consistency using CLIP-SIM [29] and DINO-SIM [27], and video quality using VBench [16] metrics. We also conduct a user study where participants rate overall preference, camera accuracy, and temporal stability.

#### 4.1. Comparison with State-of-the-Art Methods

**Baselines.** We compare our method with state-of-the-art camera-controlled video-to-video generation methods, including ReCamMaster [3], TrajectoryCrafter [46], EX4D [14], and GEN3C [31]. ReCamMaster [3] conditions a video generator on target camera poses for single-video re-rendering. TrajectoryCrafter [46] uses diffusion with point-cloud rendering guidance to follow a user-specified camera trajectory. EX4D [14] leverages a depth-watertight mesh to improve extreme-viewpoint synthesis. GEN3C [31] maintains and renders a 3D point-cloud cache

to enforce 3D-consistent camera control.

**Qualitative Results.** We present qualitative comparisons in Figs. 5, 8, and 9. In Fig. 5, we evaluate our method on two challenging scenarios: “Swing” (top) and “BMX” (bottom). As visualized in the top-left insets, these sequences pose significant challenges, including rapid foreground motion, thin structures (e.g., swing ropes), and large-scale camera displacement. The baseline methods exhibit two distinct types of failures. ReCamMaster [3] and EX4D [14] suffer from structural disintegration on fast-moving subjects, producing blurred limbs or severe ghosting artifacts as the temporal correspondence collapses. Meanwhile, TrajectoryCrafter [46] and GEN3C [31] struggle to maintain global geometric layout under large perspective shifts, leading to unnatural geometric warping and semantic drift. In contrast, our method generates high-fidelity frames with sharp details and stable geometry across both sequences. By anchoring pixels to the explicit geometry-complete 4D proxy, we effectively resolve single-view ambiguity and handle complex disocclusions—such as the background regions revealed by the biker’s motion. This ensures that the generated content remains physically plausible and temporally consistent.

Figure 8 provides additional comparisons across more diverse outdoor environments and dynamic objects. Furthermore, Fig. 9 showcases results under multiple user-specified trajectories, highlighting the flexibility and precision of our trajectory control.

**Quantitative Results.** Table 1 summarizes the quantitative comparison across automatic metrics and user ratings. On VBench, our method ranks first in five out of six dimensions, achieving the highest subject consistency (0.88), background consistency (0.94), overall consistency (0.24), aesthetic quality (0.52), and imaging quality (64). We obtain the second-best motion smoothness (0.96), slightly behind ReCamMaster (0.98), which tends to produce over-smoothed results at the cost of geometric detail. For semantic similarity and distributional fidelity, we achieve the best DINO-SIM (0.65), CLIP-SIM (0.84), and FID-V ( $1.7 \times 10^2$ ), with competitive FVD-V ( $3.6 \times 10^3$ ) on par with TrajectoryCrafter. Although they score well in Table 1, ReCamMaster and TrajectoryCrafter can still drift

from the prescribed camera path or lose 3D geometric coherence (Fig. 5). This indicates that standard automatic metrics are not sensitive to trajectory adherence, motivating our user study.

**User Study.** We conducted a user study with 20 participants to assess subjective quality across 10 diverse sequences. Participants rated results on a 1–5 scale along three axes (see the questionnaire interface in Fig. 10): (1) overall preference, (2) camera motion accuracy (adherence to the prescribed trajectory), and (3) temporal stability and source consistency (flicker and identity preservation). As shown in Table 1, our method outperforms all baselines across all axes, with particularly large margins in motion accuracy (4.5 vs. 3.4 for the next best method). This validates that our geometry-complete 4D proxy provides precise camera control and structural stability that traditional metrics fail to capture, leading to a strong overall preference score of 4.6.

## 4.2. Applications

As shown in Fig. 6, FreeOrbit4D also enables several practical and interesting applications beyond camera redirection, thanks to our explicit and geometry-complete 4D representation.

**Appearance Propagation.** Our framework naturally supports propagating appearance modifications from a single edited reference frame to the entire redirected video. Using an off-the-shelf image editing model (Qwen-Image-Edit [42]), we can alter the reference frame with color changes (e.g., black-and-white stripes on the Mini Cooper) or global style transformations (e.g., anime rendering). The geometry-complete 4D proxy provides consistent depth scaffolds across all target viewpoints, enabling the video diffusion model to faithfully transfer the edited appearance throughout the sequence with temporal stability and view consistency.

**4D Geometry Manipulation.** Our explicit point-based 4D representation enables direct geometric manipulation in space-time. By modifying the point cloud, such as uniformly scaling the foreground object or compositing point clouds from different sources into a shared scene, we can synthesize plausible redirected videos from the edited 4D geometry. This capability highlights the flexibility of explicit 4D representations for intuitive scene manipulation that is difficult to achieve with purely implicit generative approaches.

## 5. Ablation Study

We conduct ablation studies to assess the contribution of each key component in our pipeline. All variants are evaluated under the same setting as our main experiments. Quantitative results are reported in Table 2, and qualitative comparisons are shown in Fig. 7.



Figure 6. **Applications enabled by FreeOrbit4D.** Our explicit 4D representation enables various downstream applications. **Top:** Appearance editing—given a single edited reference frame (e.g., zebra pattern or anime style), our geometry-complete proxy propagates the edit consistently across all novel viewpoints. **Bottom:** Geometry editing—by directly manipulating the point cloud (scaling or compositing objects from different sources), we synthesize plausible redirected videos from the modified 4D geometry.

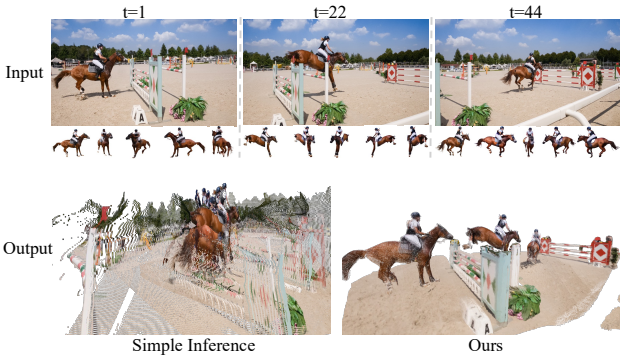


Figure 7. **Ablation: Simple Inference vs. Ours.** Directly combining multi-view images with source video in a feed-forward network leads to temporal correspondence collapse and ghosting artifacts (left). Our decoupled strategy produces a coherent 4D reconstruction (right).

**Simple Inference.** A straightforward baseline is to directly feed the multi-view images together with the source video into a dynamic-aware feed-forward reconstruction network, bypassing our decoupled reconstruction strategy. However, as shown in Fig. 7, this naive combination fails to produce a coherent 4D reconstruction: because the same object across different frames exhibits highly similar appearance, the network tends to collapse correspondences across time, resulting in severe misalignment and ghosting artifacts.

**Without Multi-View Generation (MVG).** We remove the

Table 2. **Ablation study.** We evaluate the contribution of multi-view generation (MVG) and Kalman filter smoothing (KF). **Bold**: best.

Components		DINO-SIM	FID-Sim	FID-V	FVD-V
MVG	KF	( $\uparrow$ )	( $\uparrow$ )	( $\downarrow \times 10^2$ )	( $\downarrow \times 10^3$ )
<b>X</b>	<b>X</b>	0.58	0.81	1.9	4.1
<b>✓</b>	<b>X</b>	0.60	0.82	1.9	4.1
<b>✓</b>	<b>✓</b>	<b>0.65</b>	<b>0.84</b>	<b>1.7</b>	<b>3.6</b>

multi-view generation step and rely solely on geometry-incomplete point clouds for guidance. As shown in Table 2, performance degrades across all metrics, indicating that multi-view generation provides geometry-complete structural cues that are critical for stable synthesis under large viewpoint changes.

**Without Kalman Filter (KF).** We disable the temporal smoothing module. The consistent performance drop demonstrates that Kalman filtering is important for suppressing frame-to-frame jitter and improving temporal coherence in the final output.

## 6. Conclusion

We present **FreeOrbit4D**, a training-free framework for camera redirection from a single monocular video. By reconstructing a geometry-complete 4D proxy as geometric scaffolds for video generation, our method achieves SOTA fidelity, temporal coherence, and camera control under large viewpoint changes, while enabling applications such as appearance propagation and scene manipulation. Future work may explore integrating learned priors for improved robustness and leveraging the recovered 4D proxy for downstream tasks such as 4D asset creation and data generation.

## Acknowledgments

This research is supported by the National Artificial Intelligence Research Resource (NAIRR) Pilot under award NAIRR250199. Computational resources are also provided by Delta and DeltaAI at the National Center for Supercomputing Applications (NCSA) through ACCESS allocations CIS250012, CIS250816, and CIS251188. S. W. is also supported by NSF Awards #2525287, #2404385, #2414227, #2340254, #2312102, and #2331878, and research grants from IBM, Meta, NVIDIA, and Intel.

## References

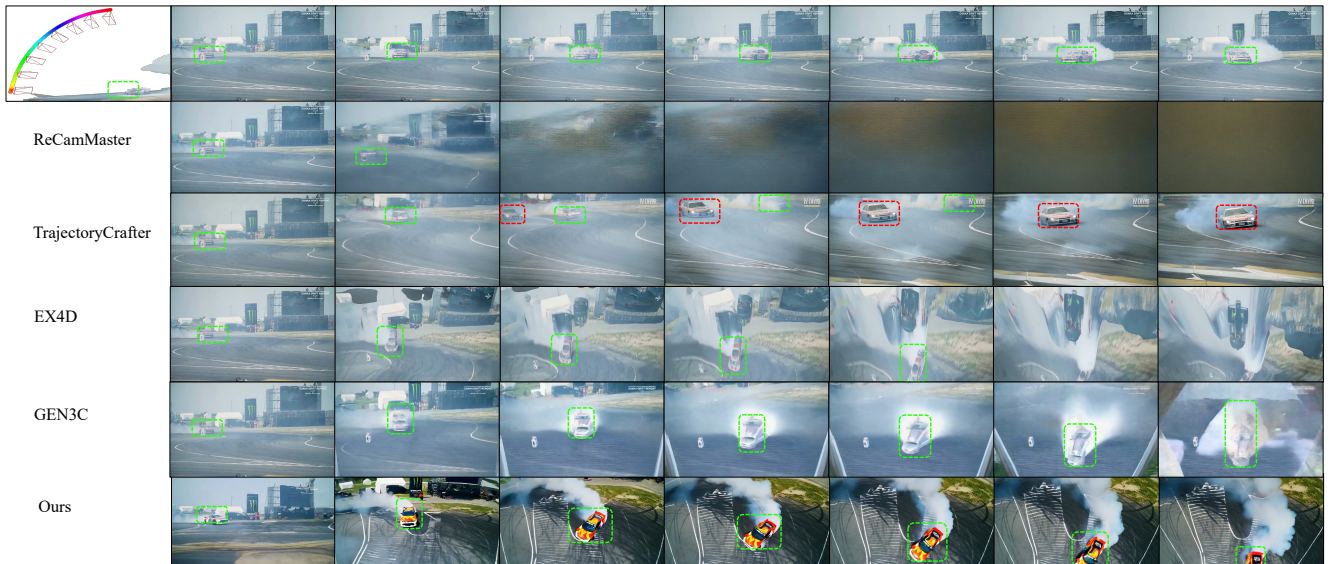
- [1] Ronald T Azuma. A survey of augmented reality. *Presence: teleoperators & virtual environments*, 6(4):355–385, 1997. 2
- [2] Sherwin Bahmani, Ivan Skorokhodov, Aliaksandr Siarohin, Willi Menapace, Guocheng Qian, Michael Vasilkovsky, Hsin-Ying Lee, Chaoyang Wang, Jiaxu Zou, Andreas Blattmann, Tim Dockhorn, Sumith Kulal, Daniel Mendelevitch, Maciej Kilian, Dominik Lorenz, Yam Levi, Zion English, Vikram Voleti, Adam Letts, et al. Recammaster: Camera-controlled generative rendering from a single video. In *ICCV*, 2025. 2, 3, 6, 7
- [3] Jianhong Bai, Menghan Xia, Xiao Fu, Xintao Wang, Lianrui Mu, Jinwen Cao, Zuozhu Liu, Haoji Hu, Xiang Bai, Pengfei Wan, et al. Recammaster: Camera-controlled generative rendering from a single video. In *ICCV*, 2025. 2, 3, 6, 7
- [4] Andreas Blattmann, Tim Dockhorn, Sumith Kulal, Daniel Mendelevitch, Maciej Kilian, Dominik Lorenz, Yam Levi, Zion English, Vikram Voleti, Adam Letts, et al. Stable video diffusion: Scaling latent video diffusion models to large datasets. *arXiv preprint arXiv:2311.15127*, 2023. 3
- [5] Yuanhao Cai, Zihao Xiao, Yixun Liang, Minghan Qin, Yulun Zhang, Xiaokang Yang, Yaoyao Liu, and Alan L Yuille. Hdr-gs: Efficient high dynamic range novel view synthesis at 1000x speed via gaussian splatting. In *NeurIPS*, 2024. 2
- [6] Wei Cao, Chang Luo, Biao Zhang, Matthias Nießner, and Jiapeng Tang. Motion2vecsets: 4D latent vector set diffusion for non-rigid shape reconstruction and tracking. In *CVPR*, 2024. 3
- [7] Wei Cao, Marcel Hallgarten, Tianyu Li, Daniel Dauner, Xunjiang Gu, Caojun Wang, Yakov Miron, Marco Aiello, Hongyang Li, Igor Gilitschenski, Boris Ivanovic, Marco Pavone, Andreas Geiger, and Kashyap Chitta. Pseudo-simulation for autonomous driving. In *CoRL*, 2025. 2
- [8] Xiang Fan, Sharath Girish, Vivek Ramanujan, Chaoyang Wang, Ashkan Mirzaei, Petr Sushko, Aliaksandr Siarohin, Sergey Tulyakov, and Ranjay Krishna. Omniview: An all-seeing diffusion model for 3d and 4d view synthesis. *arXiv preprint arXiv:2512.10940*, 2025. 3
- [9] Chen Gao, Ayush Saraf, Johannes Kopf, and Jia-Bin Huang. Dynamic view synthesis from dynamic monocular video. In *ICCV*, 2021. 2
- [10] Google DeepMind. Veo. <https://deepmind.google/models/veo/>, 2024. Accessed: 2024-11-05. 7
- [11] Hao He, Yinghao Xu, Yuwei Guo, Gordon Wetzstein, Bo Dai, Hongsheng Li, and Ceyuan Yang. Cameractrl: Enabling camera control for text-to-video generation. In *ICLR*, 2025. 2, 3
- [12] Martin Heusel, Hubert Ramsauer, Thomas Unterthiner, Bernhard Nessler, and Sepp Hochreiter. Gans trained by a two time-scale update rule converge to a local nash equilibrium. In *NeurIPS*, 2017. 7
- [13] Chen Hou and Zhibo Chen. Training-free camera control for video generation. In *ICLR*, 2025. 2, 3
- [14] Tao Hu, Haoyang Peng, Xiao Liu, and Yuwen Ma. Ex-4d: Extreme viewpoint 4d video synthesis via depth watertight mesh. *arXiv preprint arXiv:2506.05554*, 2025. 2, 3, 6, 7
- [15] Tianyu Huang, Wangguandong Zheng, Tengfei Wang, Yuhao Liu, Zhenwei Wang, Junta Wu, Jie Jiang, Hui Li, Rynson WH Lau, Wangmeng Zuo, and Chuncho Guo. Voyager: Long-range and world-consistent video diffusion for explorable 3d scene generation. *arXiv preprint arXiv:2506.04225*, 2025. 3
- [16] Ziqi Huang, Yinan He, Jiashuo Yu, Fan Zhang, Chenyang Si, Yuming Jiang, Yuanhan Zhang, Tianxing Wu, Qingyang Jin, Nattapol Chanpaisit, et al. Vbench: Comprehensive benchmark suite for video generative models. In *CVPR*, 2024. 7

- [17] Zeyinzi Jiang, Zhen Han, Chaojie Mao, Jingfeng Zhang, Yulin Pan, and Yu Liu. Vace: All-in-one video creation and editing. In *ICCV*, 2025. 5, 7
- [18] Bernhard Kerbl, Georgios Kopanas, Thomas Leimkühler, and George Drettakis. 3D gaussian splatting for real-time radiance field rendering. *TOG*, 2023. 2, 3
- [19] Weijie Kong, Qi Tian, Zijian Zhang, Rox Min, Zuozhuo Dai, Jin Zhou, Jiangfeng Xiong, Xin Li, Bo Wu, Jianwei Zhang, et al. Hunyuanyvideo: A systematic framework for large video generative models. *arXiv preprint arXiv:2412.03603*, 2024. 3
- [20] Rui long Li, Brent Yi, Junchen Liu, Hang Gao, Yi Ma, and Angjoo Kanazawa. Cameras as relative positional encoding. In *NeurIPS*, 2025. 3
- [21] Teng Li, Guangcong Zheng, Rui Jiang, Shuigen Zhan, Tao Wu, Yehao Lu, Yining Lin, and Xi Li. Realcam-i2v: Real-world image-to-video generation with interactive complex camera control. In *ICCV*, 2025. 2, 3
- [22] Tianqi Liu, Zhaoxi Chen, Zihao Huang, Shaocong Xu, Saining Zhang, Chongjie Ye, Bohan Li, Zhiguo Cao, Wei Li, Hao Zhao, et al. Light-x: Generative 4d video rendering with camera and illumination control. *arXiv preprint arXiv:2512.05115*, 2025. 3
- [23] Yawen Luo, Jianhong Bai, Xiaoyu Shi, Menghan Xia, Xintao Wang, Pengfei Wan, Di Zhang, Kun Gai, and Tianfan Xue. Camclone master: Enabling reference-based camera control for video generation. *arXiv preprint arXiv:2506.03140*, 2025. 2, 3
- [24] Wufei Ma, Qihao Liu, Jiahao Wang, Angtian Wang, Xiaodong Yuan, Yi Zhang, Zihao Xiao, Guofeng Zhang, Beijia Lu, Ruxiao Duan, Yongrui Qi, Adam Kortylewski, Yaoyao Liu, and Alan Yuille. Generating images with 3d annotations using diffusion models. In *ICLR*, 2024. 2
- [25] Ben Mildenhall, Pratul P. Srinivasan, Matthew Tancik, Jonathan T. Barron, Ravi Ramamoorthi, and Ren Ng. NeRF: Representing scenes as neural radiance fields for view synthesis, 2020. 2, 3
- [26] OpenAI. Sora: Creating video from text. <https://openai.com/index/sora/>, 2025. Accessed: 2024-11-05. 7
- [27] Maxime Oquab, Théophile Darcet, Théo Moutakanni, Huy Vo, Marc Szafraniec, Vasil Khalidov, Pierre Fernandez, Daniel Haziza, Francisco Massa, Alaeldin El-Nouby, et al. Dinov2: Learning robust visual features without supervision. *arXiv preprint arXiv:2304.07193*, 2023. 7
- [28] F. Perazzi, J. Pont-Tuset, B. McWilliams, L. Van Gool, M. Gross, and A. Sorkine-Hornung. A benchmark dataset and evaluation methodology for video object segmentation. In *CVPR*, 2016. 7
- [29] Alec Radford, Jong Wook Kim, Chris Hallacy, Aditya Ramesh, Gabriel Goh, Sandhini Agarwal, Girish Sastry, Amanda Askell, Pamela Mishkin, Jack Clark, et al. Learning transferable visual models from natural language supervision. In *ICML*, 2021. 7
- [30] Nikhila Ravi, Valentin Gabeur, Yuan-Ting Hu, Ronghang Hu, Chaitanya Ryali, Tengyu Ma, Haitham Khedr, Roman Rädle, Chloe Rolland, Laura Gustafson, Eric Mintun, Junting Pan, Kalyan Vasudev Alwala, Nicolas Carion, Chao-Yuan Wu, Ross Girshick, Piotr Dollár, and Christoph Feichtenhofer. Sam 2: Segment anything in images and videos. In *ICLR*, 2025. 4, 7
- [31] Xuanchi Ren, Tianchang Shen, Jiahui Huang, Huan Ling, Yifan Lu, Merlin Nimier-David, Thomas Müller, Alexander Keller, Sanja Fidler, and Jun Gao. Gen3c: 3d-informed world-consistent video generation with precise camera control. In *CVPR*, 2025. 2, 3, 6, 7
- [32] Chenxi Song, Yanming Yang, Tong Zhao, Ruibo Li, and Chi Zhang. Worldforge: Unlocking emergent 3d/4d generation in video diffusion model via training-free guidance. *arXiv preprint arXiv:2509.15130*, 2025. 3
- [33] Fengrui Tian, Jiawei Fan, Xie Yu, Shaoyi Du, Meina Song, and Yu Zhao. TCVM: Temporal contrasting video montage framework for self-supervised video representation learning. In *ACCV*, 2022. 3
- [34] Fengrui Tian, Shaoyi Du, and Yueqi Duan. MonoNeRF: Learning a generalizable dynamic radiance field from monocular videos. In *ICCV*, 2023. 2, 3
- [35] Fengrui Tian, Yueqi Duan, Angtian Wang, Jianfei Guo, and Shaoyi Du. Semantic Flow: Learning semantic fields of dynamic scenes from monocular videos. In *ICLR*, 2024. 3
- [36] Fengrui Tian, Tianjiao Ding, Jinqi Luo, Hancheng Min, and René Vidal. Voyaging into perpetual dynamic scenes from a single view. In *ICCV*, 2025. 3
- [37] Thomas Unterthiner, Sjoerd Van Steenkiste, Karol Kurach, Raphaël Marinier, Marcin Michalski, and Sylvain Gelly. Fvd: A new metric for video generation. In *ICLR*, 2019. 7
- [38] Basile Van Hoorick, Rundi Wu, Ege Ozguroglu, Kyle Sargent, Ruoshi Liu, Pavel Tokmakov, Achal Dave, Changxi Zheng, and Carl Vondrick. Generative camera dolly: Extreme monocular dynamic novel view synthesis. In *ECCV*, 2024. 3
- [39] Team Wan, Ang Wang, Baole Ai, Bin Wen, Chaojie Mao, Chen-Wei Xie, Di Chen, Feiwei Yu, Haiming Zhao, Jianxiao Yang, Jianyuan Zeng, Jiayu Wang, Jingfeng Zhang, Jingen Zhou, Jinkai Wang, Jixuan Chen, Kai Zhu, Kang Zhao, Keyu Yan, Lianghua Huang, Mengyang Feng, Ningyi Zhang, Pandeng Li, Pingyu Wu, Ruihang Chu, Ruili Feng, Shiwei Zhang, Siyang Sun, Tao Fang, Tianxing Wang, Tianyi Gui, Tingyu Weng, Tong Shen, Wei Lin, Wei Wang, Wei Wang, Wenmeng Zhou, Wente Wang, Wenting Shen, Wenyuan Yu, Xianzhong Shi, Xiaoming Huang, Xin Xu, Yan Kou, Yangyu Lv, Yifei Li, Yijing Liu, Yiming Wang, Yingya Zhang, Yitong Huang, Yong Li, You Wu, Yu Liu, Yulin Pan, Yun Zheng, Yuntao Hong, Yupeng Shi, Yutong Feng, Zeyinzi Jiang, Zhen Han, Zhi-Fan Wu, and Ziyu Liu. Wan: Open and advanced large-scale video generative models. *arXiv preprint arXiv:2503.20314*, 2025. 3, 5, 7
- [40] Jianyuan Wang, Minghao Chen, Nikita Karaev, Andrea Vedaldi, Christian Rupprecht, and David Novotny. Vggt: Visual geometry grounded transformer. In *CVPR*, 2025. 3, 4, 7
- [41] Zhouxia Wang, Ziyang Yuan, Xintao Wang, Yaowei Li, Tianshui Chen, Menghan Xia, Ping Luo, and Ying Shan.

- Motionctrl: A unified and flexible motion controller for video generation. In *SIGGRAPH*, 2024. 3
- [42] Chenfei Wu, Jiahao Li, Jingren Zhou, Junyang Lin, Kaiyuan Gao, Kun Yan, Sheng-ming Yin, Shuai Bai, Xiao Xu, Yilei Chen, et al. Qwen-image technical report. *arXiv preprint arXiv:2508.02324*, 2025. 8
- [43] Yiming Xie, Chun-Han Yao, Vikram Voleti, Huaizu Jiang, and Varun Jampani. Sv4d: Dynamic 3d content generation with multi-frame and multi-view consistency. In *ICLR*, 2025. 3
- [44] Zhuoyi Yang, Jiayan Teng, Wendi Zheng, Ming Ding, Shiyu Huang, Jiazheng Xu, Yuanming Yang, Wenyi Hong, Xiaohan Zhang, Guanyu Feng, et al. CogVideoX: Text-to-video diffusion models with an expert transformer. In *ICLR*, 2024. 3
- [45] Chun-Han Yao, Yiming Xie, Vikram Voleti, Huaizu Jiang, and Varun Jampani. SV4D2.0: Enhancing spatio-temporal consistency in multi-view video diffusion for high-quality 4d generation. In *ICCV*, 2025. 4, 7
- [46] Mark Yu, Wenbo Hu, Jinbo Xing, and Ying Shan. Trajectorycrafter: Redirecting camera trajectory for monocular videos via diffusion models. In *ICCV*, 2025. 2, 3, 6, 7
- [47] Wangbo Yu, Jinbo Xing, Li Yuan, Wenbo Hu, Xiaoyu Li, Zhipeng Huang, Xiangjun Gao, Tien-Tsin Wong, Ying Shan, and Yonghong Tian. Viewcrafter: Taming video diffusion models for high-fidelity novel view synthesis. *arXiv preprint arXiv:2409.02048*, 2024. 2, 3
- [48] Hao Zhang, Chun-Han Yao, Simon Donne, Narendra Ahuja, and Varun Jampani. Stable part diffusion 4d: Multi-view rgb and kinematic parts video generation. In *NeurIPS*, 2025. 2
- [49] Lvmin Zhang, Anyi Rao, and Maneesh Agrawala. Adding conditional control to text-to-image diffusion models. In *ICCV*, 2023. 3
- [50] Songchun Zhang, Huiyao Xu, Sitong Guo, Zhongwei Xie, Pengwei Liu, Hujun Bao, Weiwei Xu, and Changqing Zou. Spatialcrafter: Unleashing the imagination of video diffusion models for scene reconstruction from limited observations. In *ICCV*, 2025. 3
- [51] Yanran Zhang, Ziyi Wang, Wenzhao Zheng, Zheng Zhu, Jie Zhou, and Jiwen Lu. Joint 3d geometry reconstruction and motion generation for 4d synthesis from a single image. *arXiv preprint arXiv:2512.05044*, 2025. 3
- [52] Hongkuan Zhou, Wei Cao, Aifen Sui, and Zhenshan Bing. What matters to enhance traffic rule compliance of imitation learning for end-to-end autonomous driving. *arXiv preprint arXiv:2309.07808*, 2023. 2
- [53] Hongkuan Zhou, Stefan Schimid, Yicong Li, Lavdim Halilaj, Xiangtong Yao, and Wei Cao. Predicting the road ahead: A knowledge graph based foundation model for scene understanding in autonomous driving. In *European Semantic Web Conference*, 2025. 2
- [54] Kaichen Zhou, Yuhang Wang, Grace Chen, Xinhai Chang, Gaspard Beaudouin, Fangneng Zhan, Paul Pu Liang, and Mengyu Wang. Page-4d: Disentangled pose and geometry estimation for 4d perception. *arXiv preprint arXiv:2510.17568*, 2025. 3, 4, 7

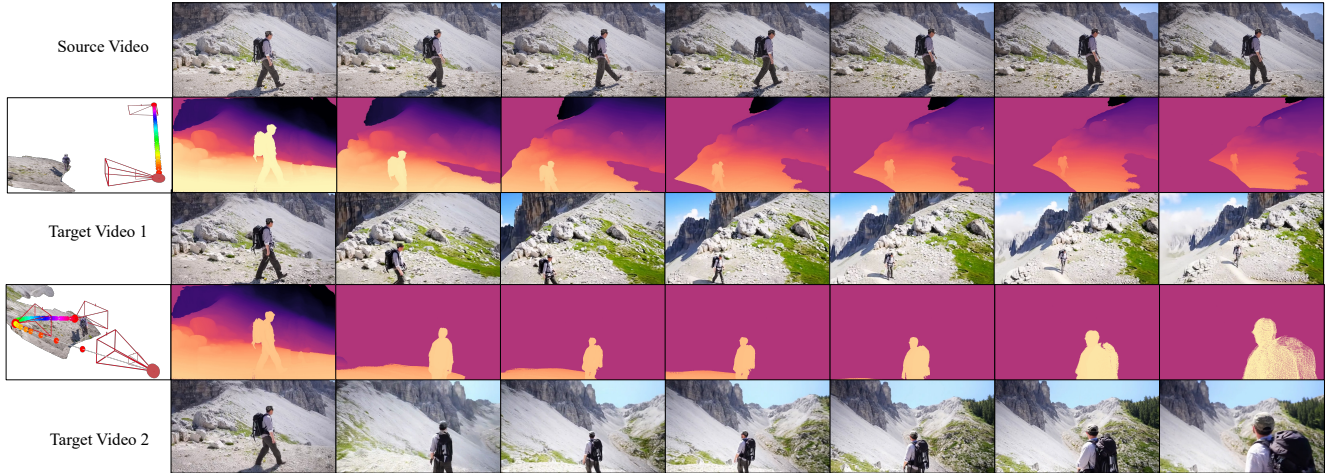


(a) Qualitative comparison on the “Camel” sequence.



(b) Qualitative comparison on “Drift”.

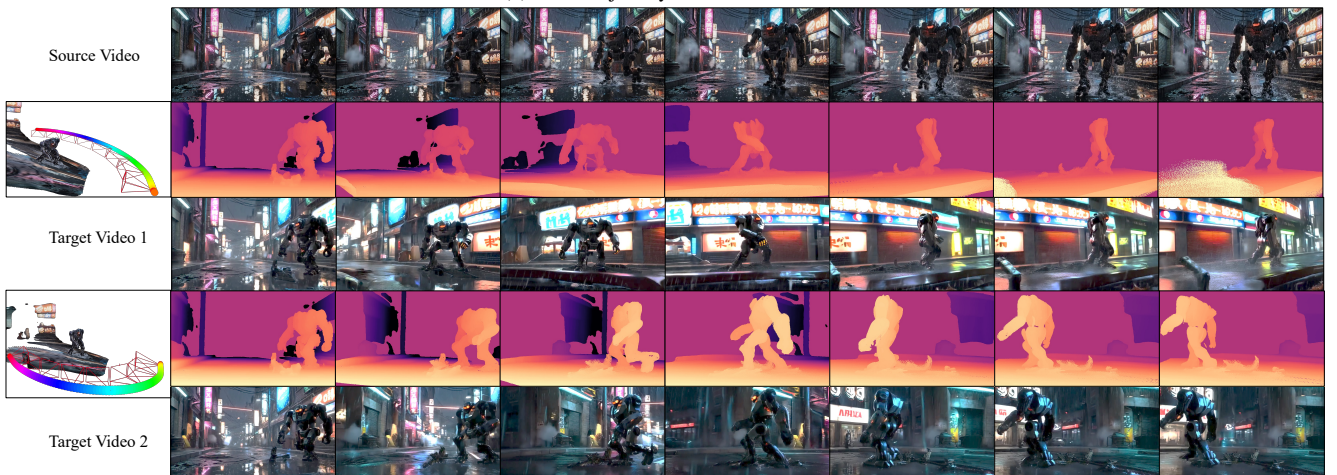
Figure 8. **Additional qualitative comparisons on various sequences.** Compared to baseline methods, which suffer from geometric distortions, motion blur, and semantic drift under large viewpoint changes, our method produces consistently sharp textures and stable geometry. These results demonstrate the effectiveness of our geometry-complete 4D proxy in handling fast motion and complex backgrounds.



(a) Multi-trajectory results on “Hike”.



(b) Multi-trajectory results on “Bear”.



(c) Multi-trajectory results on “Robot”.

**Figure 9. Multi-trajectory video synthesis results.** We show that our method generates temporally and geometrically consistent videos along diverse target camera trajectories. By leveraging the geometry-complete 4D proxy, our approach effectively handles articulated motion, complex lighting, and thin structures across all sequences.

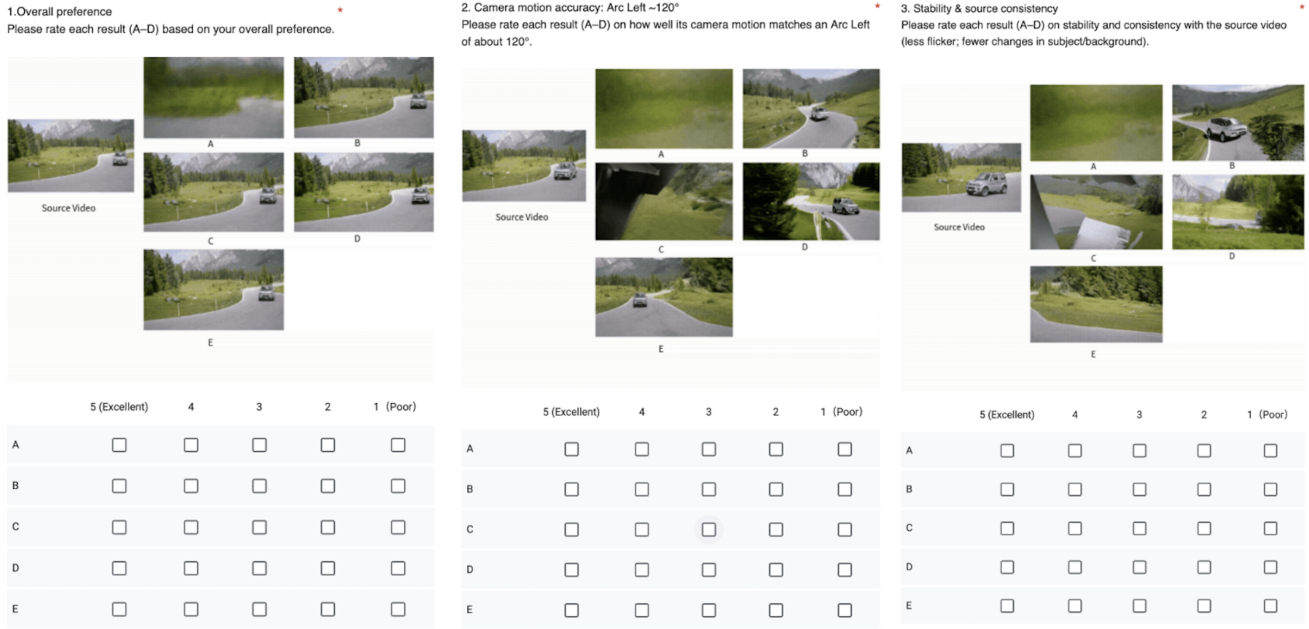


Figure 10. **User study interface.** We present the participants with two anonymized videos (ours vs. baseline) and ask them to select the one with superior temporal stability and geometric fidelity.